

Meson-exchange Currents and Quasielastic Neutrino Cross Sections

**M.B. Barbaro¹, J.E. Amaro², J.A. Caballero³, T.W. Donnelly⁴,
J.M. Udías⁵, C.F. Williamson⁶**

¹Università di Torino, 10125 Turin, Italy

²Universidad de Granada, 18071 Granada, Spain

³Universidad de Sevilla, 41080 Sevilla, Spain

^{4,6}Massachusetts Institute of Technology, Cambridge, MA 02139, USA

⁵Universidad Complutense de Madrid, 28040 Madrid, Spain

Abstract. We illustrate and discuss the role of meson-exchange currents in quasielastic neutrino-nucleus scattering induced by charged currents, comparing the results with the recent MiniBooNE data for differential and integrated cross sections.

1 Introduction

The double differential quasielastic cross section for the charged-current quasielastic (CCQE) neutrino-nucleus process has been recently measured for the first time by the MiniBooNE collaboration at Fermilab [1]. Unexpectedly, the data turned out to be substantially underestimated by the relativistic Fermi gas (RFG) model used in the experimental analysis, as well as by several more realistic nuclear models. Indeed a phenomenological model based on electron scattering data, the super-scaling approach (SuSA) [2], which describes by construction the world data on quasielastic electron scattering, yields cross sections which are lower than the RFG predictions and therefore in worse agreement with the neutrino data.

This outcome has been initially ascribed [1] to an anomalously large value of the nucleon axial mass M_A , namely the cutoff parameter entering the dipole axial form factor: in order to fit the data within the RFG model a value $M_A = 1.35 \text{ GeV}/c^2$ is required, significantly larger than the universally accepted value $M_A \simeq 1 \text{ GeV}/c^2$ [3]. An even larger axial mass would be required in the SuSA model. Similar results are found in the context of microscopical models such as the ones based on relativistic mean field theory [4, 5] or realistic structure functions [6], which have been widely tested against electron scattering.

However, as stressed in Ref. [2], effects from meson exchange currents and their associated correlations are not accounted for in the SuSA approach, since they violate scaling of both kinds- that is, the corresponding superscaling function does depend on the momentum transfer and on the nuclear target, as shown in

Refs. [7–9] - and were therefore ignored in analyzing the electron scattering data in terms of superscaling. Although the effect of two-body currents is not very sizable at the quasielastic peak in electron scattering, it can be more significant in quasielastic neutrino scattering due to the different kinematical conditions. In fact in this case the neutrino beam is not monochromatic, but a wide energy range is spanned by the neutrino flux (from 0 to 3 GeV for MiniBooNE): an event is classified as “quasielastic” if no pions are present in the final state, but it does not necessarily correspond to one-nucleon knockout. In the calculations of Refs. [10] and [11] it has been shown that multinucleon channels can account for the behavior of the CCQE cross sections without need of an anomalously large axial mass. On the other hand a different model, based on the relativistic Green’s function framework, is also able to describe the experimental without the need to modify the nucleon axial mass, as recently shown on Ref. [12]. Hence, before drawing any conclusion on the nucleon axial mass as extracted from neutrino data, a careful evaluation of all nuclear effects and of the relevance of multinucleon emission and of some non-nucleonic contributions is required.

A further point we would like to stress is that the kinematics of ongoing and future neutrino experiments demands relativity as an essential ingredient and traditional non-relativistic models are questionable in this regime. Here we shall present a fully relativistic model for the meson exchange currents (MEC) associated to the pion and discuss the corresponding results for both electron and neutrino reactions. Further details and results can be found in Refs. [7, 8, 13–15].

2 Meson Exchange Currents

Meson exchange currents are two-body currents carried by a virtual meson exchanged between two nucleons in the nucleus. The MEC considered in this work are represented by the Feynman diagrams of Fig. 1, where the dashed line represents a pion.

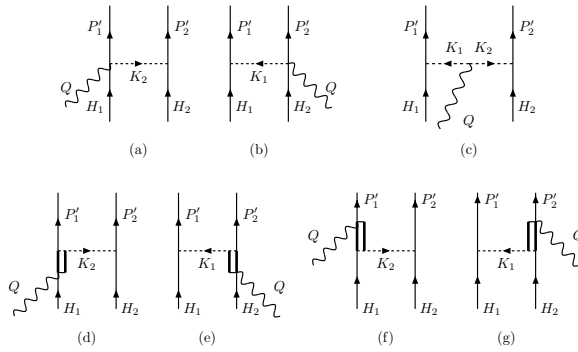


Figure 1. Two-body meson-exchange currents. (a) and (b): “contact”, or “seagull” diagrams; (c): “pion-in-flight” diagram; (d)-(g): “ Δ -MEC diagrams (the thick lines represent the propagator of the Δ -resonance).

Assuming pseudo-vector nucleon-pion coupling, the fully relativistic MEC matrix elements can be classified as follows [7, 8]:

1) Seagull or contact (diagrams *a-b*)

$$j_s^\mu = \frac{f^2}{m_\pi^2} i\epsilon_{3ab} \bar{u}(\mathbf{p}'_1) \tau_a \gamma_5 K_1 u(\mathbf{p}_1) \frac{F_1^V}{K_1^2 - m_\pi^2} \bar{u}(\mathbf{p}'_2) \tau_b \gamma_5 \gamma^\mu u(\mathbf{p}_2) + (1 \leftrightarrow 2).$$

2) Pion-in-flight (diagram *c*)

$$j_p^\mu = \frac{f^2}{m_\pi^2} i\epsilon_{3ab} \frac{F_\pi (K_1 - K_2)^\mu}{(K_1^2 - m_\pi^2)(K_2^2 - m_\pi^2)} \bar{u}(\mathbf{p}'_1) \tau_a \gamma_5 K_1 u(\mathbf{p}_1) \bar{u}(\mathbf{p}'_2) \tau_b \gamma_5 K_2 u(\mathbf{p}_2).$$

In the above F_1^V and F_π are the electromagnetic isovector nucleon and pion form factors, respectively and $f^2/4\pi = 0.08$ is the pion-nucleon coupling constant.

3) Δ current (diagrams *d-g*)

$$j_\Delta^\mu = \frac{f_{\pi N \Delta} f}{m_\pi^2} \frac{1}{K_2^2 - m_\pi^2} \bar{u}(\mathbf{p}'_1) T_a^\mu(1) u(\mathbf{p}_1) \bar{u}(\mathbf{p}'_2) \tau_a \gamma_5 K_2 u(\mathbf{p}_2) + (1 \leftrightarrow 2).$$

The vector $T_a^\mu(1)$ is related to the pion electroproduction amplitude

$$T_a^\mu(1) = K_{2\alpha} \Theta^{\alpha\beta} G_{\beta\rho}^\Delta (H_1 + Q) S_f^{\rho\mu} (H_1) T_a T_3^\dagger + T_3 T_a^\dagger S_b^{\mu\rho} (P'_1) G_{\rho\beta}^\Delta (P'_1 - Q) \Theta^{\beta\alpha} K_{2\alpha}$$

and involves the forward and backward Δ electroexcitation tensors:

$$\begin{aligned} S_f^{\rho\mu}(H_1) &= \Theta^{\rho\mu} (g_1 \not{Q} - g_2 H_1 \cdot Q + g_3 Q^2) \gamma_5 - \Theta^{\rho\nu} Q_\nu (g_1 \gamma^\mu - g_2 H_1^\mu + g_3 Q^\mu) \gamma_5 \\ S_b^{\rho\mu}(P'_1) &= \gamma_5 (g_1 \not{Q} - g_2 P'_1 \cdot Q - g_3 Q^2) \Theta^{\mu\rho} - \gamma_5 (g_1 \gamma^\mu - g_2 P'_1{}^\mu - g_3 Q^\mu) Q_\nu \Theta^{\nu\rho}, \end{aligned}$$

where g_i are the electromagnetic coupling constants, $\Theta_{\mu\nu} = g_{\mu\nu} - \frac{1}{4} \gamma_\mu \gamma_\nu$ and

$$G_{\beta\rho}^\Delta(P) = -\frac{P + m_\Delta}{P^2 - m_\Delta^2} \left(g_{\beta\rho} - \frac{1}{3} \gamma_\beta \gamma_\rho - \frac{2}{3} \frac{P_\beta P_\rho}{m_\Delta^2} - \frac{\gamma_\beta P_\rho - \gamma_\rho P_\beta}{3m_\Delta} \right)$$

is the Rarita-Schwinger Δ propagator. Moreover we perform the substitution $m_\Delta \rightarrow m_\Delta + \frac{i}{2} \Gamma(P)$ in the denominator of the propagator to account for the Δ decay probability. Our approach for the Δ follows, as a particular case, from the more general form of the $\gamma N \Delta$ Lagrangian of Pascalutsa *et al.* [16].

The MEC are not the only two-body operators able to induce 2p-2h excitations. The correlation operators, arising from the Feynman diagrams of Fig. 2, are of the same order as the MEC in the perturbative expansion and should be included in order to preserve the gauge invariance of the theory. Their explicit expression can be found in Ref. [7].

In the next Subsections we shall illustrate the impact of these currents in electron and neutrino scattering.

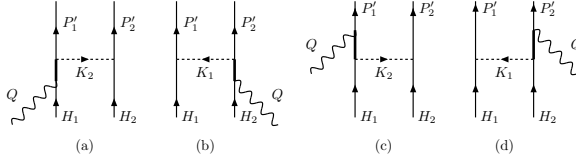


Figure 2. Two-body correlation currents.

2.1 Electron Scattering

Meson exchange currents are carried by a virtual meson which is exchanged between two nucleons in the nucleus. Being two-body currents, the MEC can excite both one-particle one-hole (1p-1h) and two-particle two-hole (2p-2h) states.

In the 1p-1h sector, MEC studies of electromagnetic (e, e') process have been performed for low-to-intermediate momentum transfers (see, *e.g.*, [7, 8, 17, 18]), showing a small reduction of the total response at the quasielastic peak, mainly due to diagrams involving the electroexcitation of the Δ resonance. However pionic correlation contributions, where the virtual boson is attached to one of the two interacting nucleons, have been shown to roughly compensate the pure MEC contribution [7, 8, 17, 18], so that in first approximation the contribution of two-body currents in the 1p-1h sector can be neglected.

In the 2p-2h sector, the contribution of pionic two-body currents to the electromagnetic response was first calculated in the Fermi gas model in Refs. [19, 20], where sizable effects were found at large energy transfers. In these references a non-relativistic reduction of the currents was performed, while fully relativistic calculations have been developed more recently in Refs. [15, 21, 22]. In [22] only the pure MEC were considered, while in [15] the correlation diagrams were also included. The latter present the problem of giving an infinite answer in a Fermi gas model, due to a nucleon propagator that can be on-shell in the region of the quasielastic peak and gives rise to a double pole inside the integral. Various prescriptions have been followed in order to avoid this problem [23–25], which is intrinsically related to the infinite extension of the Fermi gas. In Ref. [15] we have dealt with the above divergence by means a regularization parameter ϵ which accounts for the finite size of the nucleus. An exploratory study of the results has shown that a reasonable assumption for the regularization parameter, related to the propagation time of a real nucleon inside the nucleus, is $\epsilon \sim 200$ MeV, appreciably larger than the usual values of the nucleon width for collisions.

In Fig. 3 we show the transverse electromagnetic response function for the ^{56}Fe for two values of the momentum transfer, $q = 550$ and 1140 MeV/c. The contribution due to the full two-body current (MEC+correlations) in the 2p-2h sector (red, full solid) is compared with the 1p-1h response produced by the one-body current in the free relativistic Fermi gas (dashed). The separate contributions of the MEC (black, dotted) and correlations (red, thin solid) are also

shown. It appears that the MEC produce a large peak with a maximum around $\omega = (m_\Delta^2 + q^2)^{1/2} - m_N$, that comes from the Δ propagator appearing in the Δ -current. Indeed the latter turns out to dominate over the other diagrams, pion-in-flight and seagull, and to be almost negligible in the longitudinal channel. The presence of correlations leads to an additional, significant raise of the high energy tail. Moreover the correlation contribution, compared with the OB responses, is similar in the T and L channels, since its relative weight is independent of the particular component of the current (see Ref. [15]).

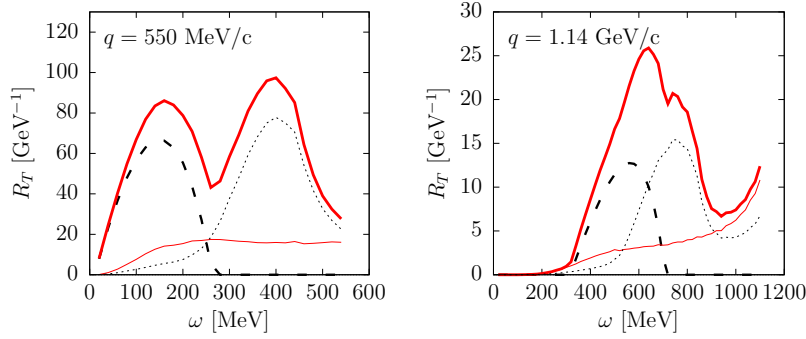


Figure 3. (Color online) Transverse response of ^{56}Fe at $q = 550$ and 1140 MeV/c. Dashed: RFG 1p-1h response with OB current only. Dotted: MEC only. Thin solid (red): Correlation only for $\epsilon = 200$ MeV. Thick solid (red): total one- plus two- body responses.

2.2 Neutrino scattering

In this section we apply the model above illustrated to CCQE neutrino scattering, implementing it in the phenomenological SuSA approach.

The CCQE neutrino-nucleus double differential cross section can be written according to a Rosenbluth-like decomposition as [2]

$$\left[\frac{d^2\sigma}{dT_\mu d\cos\theta} \right]_{E_\nu} = \sigma_0 \left[\hat{V}_L R_L + \hat{V}_T R_T + \hat{V}_{T'} R_{T'} \right], \quad (1)$$

where T_μ and θ are the muon kinetic energy and scattering angle, E_ν is the incident neutrino energy, σ_0 is the elementary cross section, \hat{V}_i are kinematic factors and R_i are the nuclear response functions, the indices L, T, T' referring to longitudinal, transverse, transverse-axial, components of the nuclear current, respectively. The response functions R_L and R_T have both “VV” and “AA” components (stemming from the product of two vector or axial currents, respectively), whereas the axial response $R_{T'}$ arises from the interference of the axial and vector nuclear currents.

The SuSA approximation consists in modifying the well-known RFG response functions by replacing the free Fermi gas parabolic scaling function with

the phenomenological scaling function f extracted from electron scattering experimental data [26, 27]. On the basis of the SuSA result, we have modified the nuclear responses according to the RFG predictions, as described in the previous section, to account for the effect of the MEC. As previously explained, we can neglect in first approximation the MEC in the 1p-1h sector and restrict our attention to 2p-2h final states. Moreover, in lowest order the MEC affect only the transverse polar vector response R_T^{VV} , since they are negligible in the longitudinal channel and suppressed in transverse axial channel.

The corresponding results are shown in Fig. 4, where the double differential CCQE cross sections obtained in the SuSA approach, with and without inclusion of MEC, are compared with the MiniBooNE data after averaging over the experimental neutrino flux. It appears the 2p-2h MEC tend to increase the cross

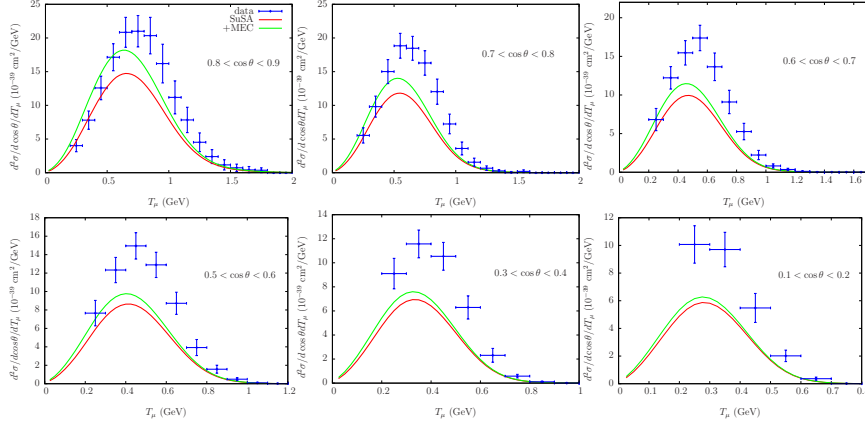


Figure 4. Flux-integrated ν_μ - ^{12}C CCQE double differential cross section per target nucleon evaluated in the SuSA model with and without inclusion of 2p2h MEC displayed versus the muon kinetic energy T_μ for various bins of the muon scattering angle $\cos\theta$. Here and in the following figures the data are from MiniBooNE [1].

section, yielding reasonable agreement with the data for not too high scattering angles (up to $\cos\theta \simeq 0.6$). At larger angles the disagreement with the experiment becomes more and more significant and the meson-exchange currents are not sufficient to account for the discrepancy.

The single differential cross sections with respect to the muon kinetic energy and scattering angle, respectively, are presented in Figs. 5 and 6, where the relativistic Fermi gas (RFG) and relativistic mean field (RMF) results are also shown for comparison: again it appears the inclusion of 2p-2h excitations leads to a good agreement with the data at high T_μ , but strength is still missing at the lower muon kinetic energies (namely higher energy transfers) and higher angles.

Finally, in Fig. 7 the fully integrated CCQE cross section per neutron is displayed versus the neutrino energy and compared with the experimental flux-unfolded data. Besides the models above discussed, we show for comparison

also the results of the relativistic mean field model when the final state interactions are ignored (denoted as RPWIA - relativistic plane wave impulse approximation) or described through a real optical potential (denoted as rROP). Note that the discrepancies between the various models, observed in Figs. 5 and 6, tend to be washed out by the integration, yielding very similar results for the models that include final state interactions (FSI) (SuSA, RMF and rROP), all of them giving a lower total cross section than the models without FSI (RFG and RPWIA). On the other hand the SuSA+MEC curve, while being closer to the data at high neutrino energies, has a somewhat different shape with respect to the other models, in qualitative agreement with the calculation of [11].

Some caution should be expressed before drawing definitive conclusions from the agreements or disagreements seen in the results. For instance, there are strong indications from RMF studies as well as from QE (e, e') data that the vector transverse response should be enhanced over the strict SuSA strategy employed here. Moreover, the correlation contributions, as shown in the previous section, are non-negligible in electron scattering when calculated in the RFG framework and should in principle be considered. However, besides the strong model dependence of these contributions, associated to the already mentioned problem of the double pole, it is difficult to implement them in the SuSA model since some correlation effects may be already accounted for by the phenomenological scaling function, and simply summing the effects of RFG-based correlation diagrams to the SuSA responses would lead to double counting. Work is in progress to consistently include the correlation contribution in a microscopic relativistic model.

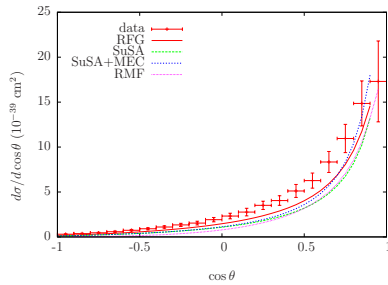


Figure 5. (Color online) Flux-averaged cross section integrated over the scattering angle and displayed versus the muon kinetic energy.

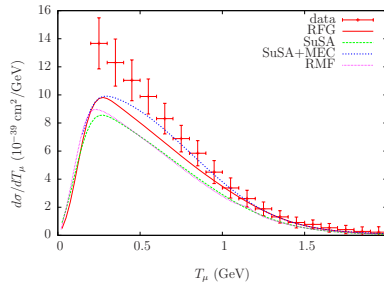


Figure 6. (Color online) Flux-averaged cross section integrated over the muon kinetic energy and displayed versus the scattering angle.

A last comment is in order concerning the comparison with the data: the average over the neutrino energy flux may require to account for effects not included in models devised for quasi-free scattering. This is, for instance, the situation at the most forward scattering angles, where a significant contribution in the cross section comes from very low-lying excitations in nuclei [13]. This is

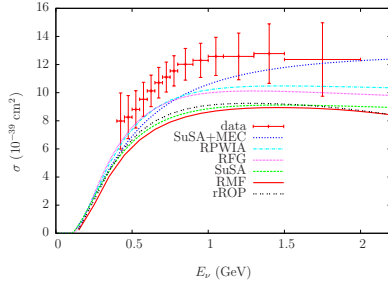


Figure 7. (Color online) Total CCQE cross section per neutron versus the neutrino energy. The curves corresponding to different nuclear models are compared with the flux unfolded MiniBooNE data [1].

clearly illustrated in Fig. 8, where the double differential cross section is evaluated in the SuSA model at the MiniBooNE kinematics and the lowest angular bin and compared with the result obtained by excluding the energy transfers lower than 50 MeV from the flux-integral. At these angles 30-40% of the cross section corresponds to very low energy transfers, where collective effects dominate and any approach based on impulse approximation is inadequate to describe the nuclear dynamics.

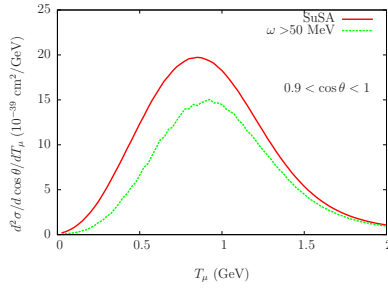


Figure 8. (Color online) Solid lines (red online): flux-integrated cross sections calculated in the SuSA model for a specific bin of scattering angle. Dashed lines (green online): a lower cut $\omega = 50$ MeV is set in the integral over the neutrino flux.

3 Conclusion

In summary, we have shown that 2p-2h meson exchange currents play an important role in CCQE neutrino scattering and may help to resolve the controversy on the nucleon axial mass raised by the recent MiniBooNE data. In our approach two-body currents arise from microscopic relativistic modeling performed for inclusive electron scattering reactions and they are known to result in a significant increase in the vector-vector transverse response function, in concert with QE electron scattering data. It should, however, be remembered that the present approach, when applied to neutrino scattering, still lacks the contributions from the correlation diagrams associated with the MEC which are required by gauge invariance; these might improve the agreement with the data, as suggested by the results for inclusive electron scattering.

References

- [1] A. A. Aguilar-Arevalo *et al.* [MiniBooNE Collaboration], *Phys. Rev.* **D81** 092005 (2010).
- [2] J. E. Amaro, M. B. Barbaro, J. A. Caballero, T. W. Donnelly, A. Molinari and I. Sick, *Phys. Rev.* **C71** 015501 (2005).
- [3] V. Bernard, L. Elouadrhiri, U. .G. Meissner, *J. Phys.* **G28** R1-R35 (2002).
- [4] J. A. Caballero, J. E. Amaro, M. B. Barbaro, T. W. Donnelly, C. Maieron and J. M. Udias, *Phys. Rev. Lett.* **95** 252502 (2005).
- [5] J. E. Amaro, M. B. Barbaro, J. A. Caballero and T. W. Donnelly, *Phys. Rev. Lett.* **98** 242501 (2007).
- [6] O. Benhar, P. Coletti, D. Meloni, *Phys. Rev. Lett.* **105** 132301 (2010).
- [7] J. E. Amaro, M. B. Barbaro, J. A. Caballero, T. W. Donnelly and A. Molinari, *Phys. Rept.* **368** 317 (2002).
- [8] J. E. Amaro, M. B. Barbaro, J. A. Caballero, T. W. Donnelly and A. Molinari, *Nucl. Phys.* **A723** 181 (2003).
- [9] A. De Pace, M. Nardi, W. M. Alberico, T. W. Donnelly, A. Molinari, *Nucl. Phys.* **A741** 249-269 (2004).
- [10] M. Martini, M. Ericson, G. Chanfray, and J. Marteau, *Phys. Rev.* **C80** 065501 (2009).
- [11] J. Nieves, I. Ruiz Simo, M. J. Vicente Vacas, *Phys. Rev.* **C83** 045501 (2011).
- [12] A. Meucci, M. B. Barbaro, J. A. Caballero, C. Giusti, J. M. Udias, *Phys. Rev. Lett.* **107** 172501 (2011).
- [13] J. E. Amaro, M. B. Barbaro, J. A. Caballero, T. W. Donnelly and C. F. Williamson, *Phys. Lett.* **B696** 151 (2011).
- [14] J. E. Amaro, M. B. Barbaro, J. A. Caballero, T. W. Donnelly and A. Molinari, *Nucl. Phys.* **A643** 349 (1998).
- [15] J. E. Amaro, C. Maieron, M. B. Barbaro, J. A. Caballero and T. W. Donnelly, *Phys. Rev.* **C82** 044601 (2010).
- [16] V. Pascalutsa and O. Scholten, *Nucl. Phys.* **A 591** 658 (1995).
- [17] W. M. Alberico, T. W. Donnelly and A. Molinari, *Nucl. Phys.* **A512** 541 (1998).
- [18] J. E. Amaro, M. B. Barbaro, J. A. Caballero, T. W. Donnelly, C. Maieron and J. M. Udias, *Phys. Rev.* **C81** 014606 (2010).
- [19] T. W. Donnelly, J. W. Van Orden, T. De Forest, Jr., W. C. Hermans, *Phys. Lett.* **B76**, 393 (1978).
- [20] J. W. Van Orden, T. W. Donnelly, *Annals Phys.* **131**, 451-493 (1981).
- [21] M.J. Dekker, P.J. Brussaard, and J.A. Tjon, *Phys. Rev. C* 49 (1994) 2650.
- [22] A. De Pace, M. Nardi, W. M. Alberico, T. W. Donnelly and A. Molinari, *Nucl. Phys.* **A 726**, 303 (2003).
- [23] W. M. Alberico, M. Ericson and A. Molinari, *Ann. Phys.* **154** 356 (1984).
- [24] W. M. Alberico, A. De Pace, A. Drago and A. Molinari, *Riv. Nuov. Cim.* **14** n.5, 1 (1991).
- [25] A. Gil, J. Nieves and E. Oset, *Nucl. Phys.* **A627** 543 (1997).
- [26] D. B. Day, J. S. McCarthy, T. W. Donnelly and I. Sick, *Ann. Rev. Nucl. Part. Sci.* **40** 357 (1990).
- [27] J. Jourdan, *Nucl. Phys.* **A603** 117 (1996).